Mineralogical Magazine, October 2015, Vol. 79(5), pp. 1143–1157

Pilawite-(Y), $Ca_2(Y,Yb)_2[Al_4(SiO_4)_4O_2(OH)_2]$, a new mineral from the Piława Górna granitic pegmatite, southwestern Poland: mineralogical data, crystal structure and association

Adam Pieczka[1,*], Frank C. Hawthorne[2], Mark A. Cooper[2], Eligiusz Szełęg[3], Adam Szuszkiewicz[4], Krzysztof Turniak[4], Krzysztof Nejbert[5] and Sławomir Ilnicki[5]

[1] AGH University of Science and Technology, Department of Mineralogy, Petrography and Geochemistry 30–059 Kraków, Mickiewicza 30, Poland
[2] Department of Geological Sciences, University of Manitoba, Winnipeg, Manitoba R3T 2N2, Canada
[3] University of Silesia, Faculty of Earth Sciences, Department of Geochemistry, Mineralogy and Petrography, 41–200 Sosnowiec, Będzińska 60, Poland
[4] University of Wrocław, Institute of Geological Sciences, 50–204 Wrocław, pl. M. Borna 9, Poland
[5] University of Warsaw, Faculty of Geology, Institute of Geochemistry, Mineralogy and Petrology, 02–089 Warszawa, Żwirki and Wigury 93, Poland

[*Received 26 August 2014; Accepted 03 March 2015; Associate Editor: S.J. Mills*]

ABSTRACT

Pilawite-(Y), ideally $Ca_2(Y,Yb)_2Al_4(SiO_4)_4O_2(OH)_2$, was discovered in a pegmatite near Piława Górna, Lower Silesia, Poland. The mineral occurs as white, translucent, brittle crystals up to 1.5 mm in size. It has a white streak, vitreous lustre and a hardness of 5 on Mohs scale. The calculated density is 4.007 g/cm^3. Pilawite-(Y) is non-pleochroic, biaxial (+), with refractive indices $\alpha = 1.743(5)$, $\beta = 1.754(5)$ and $\gamma = 1.779(5)$, birefringence $\Delta = 0.03–0.04$, $2V_{meas.} = 65(2)°$ and $2V_{calc.} = 68°$. Pilawite-(Y) is monoclinic $P2_1/c$, with unit-cell parameters $a = 8.558(3)$ Å, $b = 7.260(3)$ Å, $c = 11.182(6)$ Å, $\beta = 90.61(4)°$, $V = 694.7(4)$ Å^3. The crystal structure was refined to an R1 index of 2.76% and consists of chains of edge- and corner-sharing octahedra decorated by tetrahedra and having the stoichiometry $[Al_2(SiO_4)_4O(OH)]$ that link by sharing corners to form an octahedron–tetrahedron framework with large interstices that contain Ca^{2+} and $(Y,Ln)^{3+}$. It is a graphical isomer of the Al–P framework in palermoite, $Sr_2Li_4[Al_2(PO_4)_2(OH)_2]_2$. The pilawite-(Y)-bearing assemblage began crystallization at high Y + Ln activities and was modified progressively by a Ca-enriched fluid, resulting in the sequence: keiviite-(Y) → gadolinite-(Y) to hingganite-(Y) + hellandite-(Y) → pilawite-(Y) → allanite-(Y) → epidote/zoisite.

Keywords: pilawite-(Y), new mineral species, optical data, electron microprobe, crystal structure, NYF pegmatite, Piława Górna, Poland.

Introduction

Pilawite-(Y), endmember composition $Ca_2(Y,Yb)_2Al_4(SiO_4)_4O_2(OH)_2$, was discovered in a granitic pegmatite at Piława Górna in Lower Silesia, Poland. Together with keiviite-(Y), gadolinite-(Y), hingganite-(Y) and hellandite-(Y), it forms inclusions in accessory allanite-(Y) within the blocky feldspar zone of a weakly zoned and weakly fractionated dyke that is part of cogenetic pegmatites known as the Julianna pegmatitic system (Szuszkiewicz *et al.*, 2013). During routine electron microprobe studies, attention was drawn to pilawite-(Y) due to a different ratio of Ca–*REE*–Al–Si components, i.e. 1:1:2:2 instead of 1:1:2:3, which is typical of allanite compositions. Pilawite-(Y) has been approved by the Commission on New Minerals, Nomenclature and Classification

* E-mail: pieczka@agh.edu.pl
DOI: 10.1180/minmag.2015.079.5.09

(CNMNC) of the International Mineralogical Association (IMA 2013–125). The name of the mineral is for the type locality, Piława Górna, in Lower Silesia, Poland. The holotype is preserved at the Mineralogical Museum of the University of Wrocław, Poland, in the form of one polished 1-inch disc with the catalogue number MMWr IV7676. In the Strunz system (Strunz and Nickel, 2001) pilawite-(Y) is classified in the 09.AG group, i.e. Nesosilicates with additional anions; cations in > [6] ± [6] coordination, and in Dana class 52, subclass 52.04, i.e. Nesosilicates: Nesosilicate Insular SiO_4 Groups and O, OH, F and H_2O with cations in [6] and/or > [6] coordination. The Al–Si framework of pilawite-(Y) is a graphical isomer of the Al–P framework in palermoite, $Sr_2Li_4[Al_2(PO_4)_2(OH)_2]_2$.

Geological setting

The Julianna pegmatitic system is exposed in the amphibolite–migmatite quarry of the Dolnośląskie Surowce Skalne S.A Company near the town of Piława Górna (50°42′11.77″N; 16°44′12.36″E), ~50 km southwest of Wrocław, southwest Poland. The pegmatites intruded into the rocks of the Góry Sowie Block (GSB), a tectono-stratigraphic unit (~650 km^2) located in the Sudetes, the northeastern-most exposed part of the European Variscides. The GSB is built mainly of gneisses and migmatites with minor amphibolites, and is interpreted as a fragment of the lower crust (for details see Mazur *et al*., 2006). The complex is a product of prolonged and polystadial metamorphism of ~385–370 Ma with tectonothermal events of amphibolite facies at temperatures of 775–910°C and a pressure of 6.5–8.5 kbar (Brueckner *et al*., 1996; O'Brien *et al*., 1997; Kryza and Fanning, 2007), which triggered anatectic melting in deep crustal levels and led to comprehensive migmatization, metamorphic segregation and subsequent injections of granitic magma during decompression stages, as small concordant segregations and north-trending discordant pegmatite dykes (van Breemen *et al*., 1988; Żelaźniewicz, 1990; Bröcker *et al*., 1998; Timmermann *et al*., 2000; Aftalion and Bowes, 2002; Gordon *et al*., 2005).

Although the GSB pegmatites were classified tentatively by Novák (2005) as the beryl subtype of the LCT (Li–Cs–Ta) petrogenetic family of Černý and Ercit (2005), the largest pegmatitic occurrence exposed in the area, the Julianna pegmatitic system, displays rather a hybrid NYF (Nb–Y–F) + LCT signature (Pieczka *et al*., 2013; Szuszkiewicz *et al*., 2013). The Julianna system consists of a series of co-genetic, differentiated pegmatites, ranging from homogeneous and relatively primitive dykes to simply zoned, NYF-affiliated bodies enriched in Nb, *REE*, Be and B, commonly weakly to moderately evolved and only scarcely attaining signs of more advanced evolution with LCT geochemical characteristics (Szuszkiewicz *et al*., 2013). The most common, less-evolved pegmatitic bodies host abundant rare-element-bearing mineralization, mainly in the form of (Fe,Mn)–(Ti,Sn)–(Nb,Ta) and (*REE*,U)–(Nb,Ti,Ta) oxides, e.g. columbite-group minerals, ixiolites, ferrowodginite as well as samarskite-, euxenite-, fergusonite-group minerals and pyrochlore-supergroup minerals (Pieczka *et al*., 2013, 2014). However, with increasing fractionation, the pegmatites may display units with Li- and Cs-bearing mineralization, containing, among others, elbaite–liddicoatite–rosmannite tourmaline, pollucite, spodumene, Cs-bearing beryl and Li- and Cs-micas.

Analytical methods

Electron-microprobe analyses of pilawite-(Y) and associated (Y,Ln)-bearing minerals were undertaken at the Inter-Institute Analytical Complex for Minerals and Synthetic Substances of the University of Warsaw with a CAMECA SX 100 electron microprobe operating in wavelength dispersive spectroscopy (WDS) mode with an accelerating voltage of 15 kV, a beam current of 70 nA, peak count time of 20 s, background time of 10 s and a beam diameter of 2 μm. Standards, analytical lines, diffracting crystals and mean detection limits (wt.%) were as follows: fluorapatite – F (*K*α, TAP, 0.04) and P (*K*α, PET, 0.01), wollastonite – Ca (*K*α, PET, 0.01), diopside – Mg (*K*α, TAP, 0.01) and Si (*K*α, TAP, 0.01), rutile – Ti (*K*α, PET, 0.01), orthoclase – Al (*K*α, TAP, 0.01), hematite – Fe (*K*α, LIF, 0.02), rhodonite – Mn (*K*α, LIF, 0.02), V_2O_5 – V (*K*α, LIF, 0.02), LaB_6 – La (*L*α, PET, 0.02), CeP_5O_{14} – Ce (*L*α, PET, 0.02), PrP_5O_{14} – Pr (*L*β, LIF, 0.05), $NdGaO_3$ – (*L*β, LIF, 0.09), REE3 – Sm (*L*β, LIF, 0.09), REE2 – Eu (*L*β, LIF, 0.05), GdP_5O_{14} – Gd (*L*α, LIF, 0.03), REE4 – Tb (*L*α, LIF, 0.06) and Lu (*L*α, LIF, 0.13), REE1 – Dy (*L*β, LIF, 0.14), ErP_5O_{14} – Er (*L*α, LIF, 0.06), HoP_5O_{14} – Ho (*L*β, LIF, 0.11), TmP_5O_{14} – Tm (*L*α, LIF, 0.06), YbP_5O_{14} – Yb (*L*α, LIF, 0.06), YAG – Y (*L*α, PET, 0.03), zircon – Zr (*L*α, PET, 0.02), galena – Pb (*M*α, PET, 0.04), ThO_2 – Th (*M*α, PET, 0.04) and UO_2 – U (*M*β, PET, 0.04), where REE1–REE4 are silica glass standards containing the respective

https://doi.org/10.1180/minmag.2015.079.5.09 Published online by Cambridge University Press

TABLE 1. Mean composition of pilawite-(Y).

Constituent	wt.% (*n* = 33)	Range (wt.%)	SD (wt.%)		a.p.f.u.[1)]	SD (a.p.f.u.)
P_2O_5	0.04	0.00–0.30	0.05	P^{5+}	0.00	0.01
SiO_2	28.34	28.16–28.68	0.13	Si^{4+}	3.98	0.02
TiO_2	0.26	0.00–0.82	0.20	Ti^{4+}	0.03	0.02
Al_2O_3	23.36	22.61–23.87	0.36	Al^{3+}	3.86	0.05
Fe_2O_3 [2)]	0.72	0.00–1.18	0.33	Fe^{3+}	0.08	0.04
Y_2O_3	22.17	21.01–23.20	0.44	Y^{3+}	1.65	0.03
Gd_2O_3	0.50	0.18–0.80	0.14	Gd^{3+}	0.02	0.01
Tb_2O_3	0.21	0.09–0.33	0.06	Tb^{3+}	0.01	< 0.01
Dy_2O_3	2.13	1.35–2.83	0.37	Dy^{3+}	0.10	0.02
Ho_2O_3	0.54	0.31–0.78	0.12	Ho^{3+}	0.02	0.01
Er_2O_3	2.04	1.60–2.44	0.23	Er^{3+}	0.09	0.01
Tm_2O_3	0.34	0.17–0.47	0.08	Tm^{3+}	0.02	< 0.01
Yb_2O_3	2.53	1.38–3.75	0.66	Yb^{3+}	0.11	0.03
Lu_2O_3	0.47	0.30–0.75	0.10	Lu^{3+}	0.02	< 0.01
FeO [2)]	0.32	0.00–1.06	0.35	Fe^{2+}	0.04	0.04
MnO	0.75	0.59–1.34	0.14	Mn^{2+}	0.09	0.02
CaO	12.50	11.66–13.37	0.40	Ca^{2+}	1.88	0.06
PbO	0.18	0.12–0.28	0.04	Pb^{2+}	0.01	< 0.01
H_2O [2)]	2.14	2.11–2.16	0.01	OH^-	2.00	0.00
Total	99.55	98.80–101.12		O^{2-}	18.00	

La, Ce, Pr, Nd, Sm, U, Th, Mg, As, V and F are below detection limits. SD – standard deviation.
[1)] Normalized on the basis of 18O + 2OH p.f.u. and the total of cations equal to 12 p.f.u.
[2)] Calculated from stoichiometry.

lanthanides (Drake and Weill, 1972). The raw data were reduced with the *'PAP'* routine of Pouchou and Pichoir (1985), and the overlaps of Ln analytical lines were corrected using the coefficients of Reed and Buckley (1998).

The pilawite-(Y) formula was calculated for the mean composition of 33 spot analyses on the basis of 20 O atoms per formula unit (a.p.f.u.) (18 O^{2-} + 2 OH^-) in accord with the results of structural analysis, maintaining the total number of cations equal to 12 p.f.u. by adjusting the Fe^{3+}/Fe_{total} ratio. The data and the statistics of the analytical results are presented in Table 1. H_2O was calculated by stoichiometry to 2 OH^- p.f.u. The formulae of associated phases were normalized on the basis of 7 O a.p.f.u. for keiviite-(Y) assuming $Fe_{total} = Fe^{3+}$;

TABLE 2*a*. Mean compositions (wt.%) of Y-bearing minerals associated with pilawite-(Y)

	Kvt *n* = 11	Gad *n* = 5	Hng *n* = 4	Hel *n* = 10	Aln *n* = 8	Ep *n* = 5
P_2O_5	0.06	0.05	0.04	b.d.l.	0.04	0.05
SiO_2	31.12	24.46	27.75	23.54	34.04	38.43
TiO_2	b.d.l.	b.d.l.	b.d.l.	0.13	0.03	0.07
UO_2	b.d.l.	b.d.l.	b.d.l.	b.d.l.	0.06	b.d.l.
Al_2O_3	b.d.l.	b.d.l.	b.d.l.	4.33	21.06	26.07
Fe_2O_3				0.68	1.90	8.79
Mn_2O_3				0.18		
Y_2O_3	46.54	37.09	33.19	27.61	11.84	0.30
Gd_2O_3	0.41	1.37	0.56	0.91	1.06	b.d.l.
Tb_2O_3	0.22	0.40	0.20	0.30	0.29	b.d.l.

(continued)

https://doi.org/10.1180/minmag.2015.079.5.09 Published online by Cambridge University Press

TABLE 2*a*. (*contd*.)

	Kvt *n* = 11	Gad *n* = 5	Hng *n* = 4	Hel *n* = 10	Aln *n* = 8	Ep *n* = 5
Dy_2O_3	2.87	3.79	2.56	3.07	1.76	b.d.l.
Ho_2O_3	0.94	0.83	0.84	0.61	0.23	b.d.l.
Er_2O_3	4.66	3.00	2.98	2.34	0.77	b.d.l.
Tm_2O_3	0.93	0.41	0.40	0.42	0.07	b.d.l.
Yb_2O_3	8.32	1.91	2.20	2.77	0.44	b.d.l.
Lu_2O_3	1.49	0.55	0.52	0.51	0.18	b.d.l.
FeO	0.08	11.24	6.20	b.d.l.	9.74	1.54
MnO	b.d.l.	0.13	0.03	1.15	1.92	0.67
CaO	b.d.l.	1.55	7.34	14.82	12.11	22.38
PbO	0.41	0.33	0.27	0.25	0.10	b.d.l.
$H_2O_{(calc.)}$		0.57	2.29	1.62	1.70	1.91
$BeO_{(calc.)}$		9.87	8.73			
$B_2O_{3(calc.)}$		0.46	3.95	13.44		
Totals	98.06	98.00	100.05	98.65	99.34	100.21

Notes: *n* – number of analyses; F, Mg, V, As, La, Ce, Pr, Nd, Sm, Eu, Th and U are below detection limits; b.d.l. – a content below detection limit. Abbreviations: Kvt – keiviite-(Y), Gad – gadolinite-(Y), Hng – hingganite-(Y), Hel – hellandite-(Y), Aln – allanite-(Y), Ep – epidote.

TABLE 2*b*. Mean compositions [a.p.f.u. [1)]] of Y-bearing minerals associated with pilawite-(Y)

	Kvt	Gad	Hng	Hel	Aln	Ep
P^{5+}	<0.01	<0.01	<0.01	0.00	<0.01	<0.01
Si^{4+}	2.00	2.00	2.00	4.03	2.99	3.02
Ti^{4+}	0.00	0.00	0.00	0.02	<0.01	<0.01
U^{4+}	0.00	0.00	0.00	0.00	<0.01	0.00
Al^{3+}	0.00	0.00	0.00	0.87	2.18	2.41
Fe^{3+}				0.09	0.13	0.52
Mn^{3+}				0.02		
Y^{3+}	1.59	1.61	1.27	2.52	0.55	0.01
Gd^{3+}	0.03	0.04	0.01	0.05	0.03	0.00
Tb^{3+}	<0.01	0.01	0.01	0.02	0.01	0.00
Dy^{3+}	0.06	0.10	0.06	0.17	0.05	0.00
Ho^{3+}	0.02	0.02	0.02	0.03	0.01	0.00
Er^{3+}	0.09	0.08	0.07	0.13	0.02	0.00
Tm^{3+}	0.02	0.01	0.01	0.02	<.0.01	0.00
Yb^{3+}	0.16	0.05	0.05	0.14	0.01	0.00
Lu^{3+}	0.03	0.01	0.01	0.03	<0.01	0.00
Fe^{2+}	<0.01	0.77	0.37	0.00	0.72	0.10
Mn^{2+}	0.00	0.01	<0.01	0.17	0.14	0.05
Ca^{2+}	0.00	0.13	0.57	2.72	1.14	1.88
Pb^{2+}	0.01	0.01	0.01	0.01	<0.01	0.00
$Be^{2+}_{(calc.)}$		1.94	1.51			
$B^{3+}_{(calc.)}$		0.06	0.49	3.97		
O^{2-}	7.00	9.69	8.90	22.15	12.00	12.00
OH^-		0.31	1.10	1.85	1.00	1.00

Notes: [1)] keiviiye-(Y) normalised in relation to 7 O a.p.f.u., gadolinite-(Y) and hingganite-(Y) to 2 Si a.p.f.u., hellandite-(Y) to 24 (O,OH) p.f.u., and epidote-supergroup minerals [allanite-(Y) and epidote] to 13 (O,OH) p.f.u. (see Methods).

https://doi.org/10.1180/minmag.2015.079.5.09 Published online by Cambridge University Press

2 Si a.p.f.u. for gadolinite-(Y) and hingganite-(Y), with $Fe_{total} = Fe^{2+}$ and H_2O calculated by stoichiometry; 24 (O,OH) p.f.u. for hellandite-(Y), with H_2O calculated by stoichiometry to $X + Y + Z + Si + B = 15$ a.p.f.u. with $Fe_{total} = Fe^{3+}$ and $Mn^{3+} = 1 - Al - Ti - Fe^{3+}$ and $X + Y = 6$ a.p.f.u., according to the crystal-chemical rules given by Oberti *et al*. (2002) for minerals of the hellandite group; and 13 (O,OH) p.f.u. for the epidote-supergroup minerals with H_2O calculated by stoichiometry to 1 OH^- and with the total number of cations fixed to 8 a.p.f.u. by adjusting the Fe^{3+}/Fe_{total} ratio. The mean compositions of the minerals are presented in Table 2.

Structural and spectroscopic studies were performed at the Department of Geological Sciences, University of Manitoba, Winnipeg, Canada. Very little material was available for the spectroscopic work and the spectra are not of high quality. The transmission Fourier transform infrared spectroscopy (FTIR) measurements were carried out using a Bruker Hyperion 2000 IR microscope equipped with a liquid nitrogen cooled MCT detector. A spectrum over the range 4000–650 cm^{-1} was obtained by averaging 100 scans with a resolution of 4 cm^{-1}, however only down to 1500 cm^{-1} is shown as the spectrum is saturated below this frequency.

The Raman spectrum was collected in back-scattered mode with a HORIBA Jobin Yvon-LabRAM ARAMIS integrated confocal micro-Raman system equipped with a 460 mm focal length spectrograph and a multichannel air-cooled (–70°C) CCD detector. A magnification of 100 × was used with an estimated spot size of 1 μm, a 1800 gr/mm grating, an excitation radiation of 532 nm and laser power between 5 and 12.5 mW. Calibration was undertaken using the 520.7 cm^{-1} line of Si.

Powder diffraction data (Table 3) were collected with a Bruker D8 Discover SuperSpeed micro-powder diffractometer with a multi-wire 2D detector using a modified Gandolfi attachment with Cu radiation ($\lambda_{CuK\alpha} = 1.54178$ Å) at 50 kV voltage and 60 mA current in two 8-hr frames, which were subsequently merged. No internal standard was used.

Single-crystal X-ray diffraction measurements were undertaken on a crystal (40 × 40 × 50 μm) attached to a tapered glass fibre and mounted on a Bruker D8 three-circle diffractometer equipped with a rotating-anode generator (Mo$K\alpha$ X-radiation), multilayer optics and an APEX-II detector. A total of 8112 intensities were collected

TABLE 3. Powder diffraction pattern for pilawite-(Y).

$I_{(meas.)}$ %	$d_{(meas.)}$ Å	$d_{(calc.)}$ Å	*h k l*
30	8.532	8.557	1 0 0
25	5.598	5.591	0 0 2
3	4.946	4.948	1 1 1
23	4.711	4.704	$\bar{1}$ 0 2
3	4.427	4.430	0 1 2
12	4.275	4.279	2 0 0
38	3.921	3.920	1 1 2
18	3.681	3.686	2 1 0
5 wk*	3.442	3.453	0 2 1
„	„	3.431	$\bar{1}$ 0 3
5	3.343	3.342	1 2 0
100	3.044	3.045	0 2 2
5	2.870	2.874	$\bar{1}$ 2 2
43	2.791	2.795	0 0 4
46	2.651	2.655	3 1 0
54	2.583	2.589	$\bar{3}$ 1 1
„	„	2.577	3 1 1
62	2.485	2.488	$\bar{2}$ 2 2
„	„	2.487	1 1 4
„	„	2.483	1 2 3
45 B*	2.408	2.408	$\bar{3}$ 1 2
33	2.246	2.243	3 2 0
7	2.216	2.215	0 2 4
42	2.147	2.149	$\bar{1}$ 2 4
„	„	2.140	1 2 4
7	2.106	2.106	2 3 0
19	2.052	2.052	4 1 0
11	2.020	2.022	$\bar{4}$ 1 1
10	1.970	1.968	2 3 2
14	1.935	1.935	$\bar{3}$ 1 4
„	„	1.933	$\bar{4}$ 1 2
11	1.913	1.916	3 1 4
9	1.844	1.845	3 3 0
14	1.815	1.815	0 4 0
15 B*	1.755	1.757	$\bar{3}$ 2 4
„	„	1.756	$\bar{3}$ 3 2
„	„	1.755	$\bar{4}$ 2 2
„	„	1.754	$\bar{1}$ 4 1
„	„	1.753	1 4 1
7 wk*	1.714	1.715	$\bar{2}$ 0 6
„	„	1.712	5 0 0
10	1.692	1.690	4 0 4
36	1.670	1.671	2 4 0
25	1.657	1.658	0 2 6
7	1.631	1.632	5 0 2
7	1.602	1.601	$\bar{5}$ 1 2
7	1.546	1.545	$\bar{3}$ 3 4
14	1.531	1.531	3 4 0
16	1.520	1.520	$\bar{4}$ 1 5

Notes: B = broad reflection, wk = weak reflection, * = not used in refinement.

https://doi.org/10.1180/minmag.2015.079.5.09 Published online by Cambridge University Press

TABLE 4. Miscellaneous information for pilawite-(Y).

a (Å)	8.571 (5)	Crystal size (μm)	40 × 40 × 50
b	7.261 (4)	Radiation	Mo*K*α
c	11.187 (6)	No. of reflections	8112
β (°)	91.00 (2)		
V (Å^3)	696.1 (7)	No. unique reflections	2045
Space group	$P2_1/c$	No. with ($F_o > 4\sigma F$)	2009
Z	2	R_{int} %	1.57
		R_1%	2.76
		wR_2%	7.04

Cell content: $2[Ca_2Y_2Al_4(SiO_4)O_2(OH)_2]$

$R_1 = \Sigma(|F_o| - |F_c|)/\Sigma|F_o|$
$wR_2 = [\Sigma w\ (F_o^2 - F_c^2)^2/\Sigma w\ (F_o^2)^2\ ]^{½}$, w = $1/[\sigma^2(F_o^2) + (0.0160\ P)^2 + 4.09\ P]$ where P = $(Max(F_o^2,0) + 2F_c^2)/3$

to 60°2θ using 4 s per 0.2° frame with a crystal-to-detector distance of 5 cm. Empirical absorption corrections (*SADABS*, Sheldrick, 2008) were applied and equivalent reflections were corrected for Lorentz, polarization and background effects, averaged and reduced to structure factors, resulting in 2045 unique reflections. The unit-cell dimensions were obtained by least-squares refinement of the positions of 6593 reflections with $I > 10\sigma I$ and are given in Table 4, together with other information pertaining to data collection and structure refinement.

All calculations were carried out with the *SHELXTL PC (Plus)* system of programs; *R* indices are of the form given in Table 4 and are expressed as percentages. The structure was solved by direct methods and refined in the space group $P2_1/c$ to convergence by full-matrix least-squares methods with anisotropic-displacement parameters for all sites except Y(2), which has a very low occupancy. At the later stages of refinement, difference-Fourier maps showed weak density maxima ~1 Å from the OH anion, which the incident bond-valence sum indicates is an OH group. The position of this maximum was entered into the structure model as a H atom and its parameters were refined with the soft constraint that the O–H distance be ~0.98 Å. The structure converged to a final *R*1 index of 2.76%. Refined atom coordinates and anisotropic-displacement parameters are listed in Table 5, selected interatomic distances are given in Table 6. A table of structure factors and a crystallographic information file have been deposited with the Principal Editor of *Mineralogical Magazine* and are available from www.minersoc.org/pages/e_journals/dep_mat_mm.html.

Parent pegmatite and paragenesis

Pilawite-(Y) occurs in a weakly-fractionated NYF-affiliated dyke of the Julianna pegmatitic system at Piława Górna. The dyke, ~1.5 m in thickness, is weakly zoned with a border zone and graphic intermediate zone of grey quartz + white feldspars and a blocky feldspar intermediate zone composed of white feldspars (to 20 cm in size) + abundant altered biotite and quartz + less-frequent muscovite sometimes intergrown with biotite in the mica books. The blocky feldspar intermediate zone passes into quartz with a generally milky core, locally passing into grey or even smoky quartz. Accessory minerals are common in the blocky feldspar zone and include black tourmaline, abundant zircon, monazite-(Ce), xenotime-(Y), single aggregates of allanite-group minerals and occasional Nb–Ta oxides (ixiolite with inclusions of cassiterite, fersmite, rutile and ilmenorutile). One aggregate of small, prismatic, olive-yellow crystals of allanite-(Y) contained a Ca–(Y + Ln)–Al–Si mineral [pilawite-(Y)], with a composition very similar to allanite-(Y), but with different atomic ratios of the components, i.e. 1:1:2:2 instead of 1:1:2:3, which is typical of allanite composition. Pilawite-(Y) occurs as an aggregate ~2 mm across, of 2–3 crystals reaching 1.5 mm long, enclosed in quartz and partly overgrown by allanite-(Y) (Fig. 1*a–d*). The assemblage of minerals that directly accompanies pilawite-(Y) includes keiviite-(Y), gadolinite-(Y), hingganite-(Y), hellandite-(Y) and xenotime-(Y). The chemistry of the minerals is presented in Table 2.

Keiviite-(Y), $(Y_{1.59}Ln_{0.41}Pb_{0.01})_{\Sigma 2.01}(Si_{2.00}O_7)$, forms crystals up to 2 mm long intergrown with

https://doi.org/10.1180/minmag.2015.079.5.09 Published online by Cambridge University Press

TABLE 5. Atom positions and displacement parameters (Å^2).

Site	x	y	z	U^{11}	U^{22}	U^{33}	U^{23}	U^{13}	U^{12}	U_{eq}
Y(1)	0.41902(3)	0.26152(5)	0.48095(5)	0.00566(14)	0.00732(16)	0.0114(3)	–0.00277(12)	0.00049(10)	–0.00058(9)	0.00812(14)
Y(2)	0.4197(12)	0.2618(16)	0.0318(18)							0.019(3)
Ca	0.07950(7)	0.51266(8)	0.25709(6)	0.0074(3)	0.0080(3)	0.0167(3)	0.0005(2)	0.0003(2)	–0.0006(2)	0.0107(2)
Si(1)	0.06470(10)	0.25341(13)	0.00078(8)	0.0066(4)	0.0068(4)	0.0091(4)	0.0002(3)	–0.0002(3)	–0.0003(3)	0.0075(2)
Si(2)	0.56915(10)	0.01834(13)	0.24744(8)	0.0075(4)	0.0074(4)	0.0095(4)	–0.0002(3)	0.0001(3)	–0.0007(3)	0.0081(2)
Al(1)	0.24535(11)	0.61551(14)	0.61563(9)	0.0072(4)	0.0072(5)	0.0094(4)	0.0005(3)	0.0006(3)	0.0001(3)	0.0079(2)
Al(2)	0.74942(11)	0.38393(14)	0.11481(9)	0.0078(5)	0.0077(5)	0.0098(5)	–0.0011(3)	–0.0005(3)	–0.0002(3)	0.0084(3)
O(1)	0.0417(3)	0.7823(4)	0.3810(2)	0.0103(11)	0.0121(11)	0.0100(11)	0.0003(9)	0.0017(8)	–0.0013(9)	0.0108(5)
O(2)	0.0449(3)	0.7687(4)	0.1189(2)	0.0097(11)	0.0109(11)	0.0103(11)	0.0002(9)	–0.0002(8)	–0.0010(9)	0.0103(5)
O(3)	0.1793(3)	0.0758(4)	0.0145(2)	0.0101(10)	0.0088(11)	0.0143(11)	0.0012(9)	0.0008(9)	0.0013(9)	0.0111(5)
O(4)	0.1929(3)	0.0811(4)	0.4873(2)	0.0111(11)	0.0084(11)	0.0142(11)	–0.0003(9)	–0.0001(9)	0.0009(9)	0.0112(5)
O(5)	0.6825(3)	0.2039(4)	0.2529(2)	0.0108(11)	0.0093(11)	0.0113(11)	–0.0002(9)	–0.0003(8)	–0.0007(9)	0.0105(5)
O(6)	0.3150(3)	0.3458(4)	0.2766(3)	0.0135(12)	0.0097(12)	0.0231(13)	0.0005(10)	0.0035(10)	–0.0010(9)	0.0154(5)
O(7)	0.4527(3)	0.0144(4)	0.1289(2)	0.0109(11)	0.0114(11)	0.0108(10)	0.0006(9)	0.0000(8)	–0.0035(9)	0.0110(5)
O(8)	0.5313(3)	0.4933(4)	0.1304(2)	0.0106(11)	0.0114(11)	0.0109(11)	0.0004(9)	0.0020(8)	0.0027(9)	0.0109(5)
O(9)	0.6719(3)	0.2433(3)	0.0008(2)	0.0082(10)	0.0087(11)	0.0110(11)	–0.0022(8)	0.0002(8)	–0.0009(8)	0.0093(5)
OH	0.1900(3)	0.0194(3)	0.2503(2)	0.0088(10)	0.0068(10)	0.0109(10)	–0.0004(8)	0.0009(8)	–0.0005(8)	0.0088(4)
H	0.233(6)	0.144(3)	0.248(5)							0.021(13)

TABLE 6. Selected interatomic distances in pilawite (Å).

Si(1)–O(1)a	1.633(3)	Si(2)–O(5)	1.662(3)
Si(1)–O(2)b	1.630(3)	Si(2)–O(6)d	1.624(3)
Si(1)–O(3)	1.627(3)	Si(2)–O(7)	1.647(3)
Si(1)–O(4)c	1.637(3)	Si(2)–O(8)d	1.638(3)
< Si(1)–O>	1.632	<Si(2)–O>	1.643
Al(1)–O(2)e	1.914(3)	Al(2)–O(1)d	1.937(3)
Al(1)–O(3)f	1.873(3)	Al(2)–O(4)h	1.903(3)
Al(1)–O(5)g	2.057(3)	Al(2)–O(5)	2.111(3)
Al(1)–O(7)f	2.015(3)	Al(2)–O(8)	2.042(3)
Al(1)–O(9)h	1.758(3)	Al(2)–O(9)	1.756(3)
Al(1)–OHf	1.865(3)	Al(2)–OHh	1.867(3)
< Al(1)–O>	1.914	<Al(2)–O>	1.936
Y(1)–O(3)f	2.405(3)	Y(2)–O(3)	2.468(3)
Y(1)–O(4)	2.342(3)	Y(2)–O(4)c	2.301(3)
Y(1)–O(6)	2.515(3)	Y(2)–O(7)	2.115(3)
Y(1)–O(7)f	2.335(3)	Y(2)–O(8)	2.218(3)
Y(1)–O(7)h	2.478(3)	Y(2)–O(8)i	2.581(3)
Y(1)–O(8)d	2.355(3)	Y(2)–O(9)	2.200(3)
Y(1)–O(8)f	2.662(3)	<Y(2)–O>	2.314
Y(1)–O(9)f	2.175(3)		
< Y(1)–O>	2.408(3)	Y(1)–Y(2)	0.59(2)
Ca–O(1)	2.424(3)		
Ca–O(1)a	2.492(3)		
Ca–O(2)	2.433(3)		
Ca–O(2)a	2.501(3)		
Ca–O(5)h	2.492(3)		
Ca–O(6)	2.433(3)		
Ca–OHj	2.310(3)		
< Ca–O>	2.441		

a: –x, y–1/2, –z + 1/2; b: –x, –y + 1, –z; c: x, –y + 1/2, z–1/2; d: –x + 1, y–1/2, –z + 1/2; e: x, –y + 3/2, z + 1/2; f: x, –y + 1/2, z + 1/2; g: –x + 1, –y + 1, –z + 1; h: –x + 1, y + 1/2, –z + 1/2; i: –x + 1, –y + 1, –z; j: –x, y + 1/2, –z + 1/2.

pilawite-(Y) and allanite-(Y), as well as numerous prismatic inclusions within pilawite-(Y). Locally, it shows poorly developed zoning with the Yb/Y ratio decreasing towards the edges of the crystals.

Gadolinite-(Y), $(Y_{1.61}Ln_{0.32}Ca_{0.06}Pb_{0.01})_{\Sigma 2.00}(Fe^{2+}_{0.77}Ca_{0.06}Mn_{0.01}\square_{0.15})_{\Sigma 1.00}[(Be_{1.94}B_{0.06})Si_2O_{9.69}(OH)_{0.31}]$, evolving to hingganite-(Y) occurs only as inclusions within pilawite-(Y). The largest inclusion, ~150 μm × 200 μm, displays a distinctly zoned texture with a patchy core of gadolinite-(Y) and a rim with compositions grading from a transitional gadolinite-(Y)–hingganite-(Y) variety to Ca-bearing hingganite-(Y), $(Y_{1.27}Ca_{0.49}Ln_{0.24}Pb_{0.01})_{\Sigma 2.00}(\square_{0.56}Fe^{2+}_{0.37}Ca_{0.07})_{\Sigma 1.00}[(Be_{1.51}B_{0.49})Si_2O_{8.90}(OH)_{1.10}]$, in the outermost zone.

Tiny inclusions of hellandite-(Y) in pilawite-(Y) do not exceed 50 μm. They display a very homogeneous composition, $(Ca_{2.72}Mn_{0.17}Pb_{0.01}Y_{1.11})_{\Sigma 4.00}(Y_{1.41}Ln_{0.59})_{\Sigma 2.00}(Al_{0.87}Fe^{3+}_{0.09}Mn^{3+}_{0.02}Ti_{0.02})_{\Sigma 1.00}\square_{2.00}[B_{3.97}Si_{4.03}O_{22.15}](OH)_{1.85}$, close to the ideal endmember formula of hellandite-(Y).

Xenotime-(Y), probably partly altered to churchite-(Y), was found as inclusions in pilawite-(Y). The host allanite-(Y) and epidote–zoisite also contain rare inclusions of xenotime-(Y) and monazite-(Ce).

Highly inhomogeneous epidote-supergroup minerals overgrow the keiviite-(Y)–pilawite-(Y)-bearing aggregate or occur within feldspar-quartz-muscovite portions of the pegmatite as rare, separate aggregates of yellowish to willow-green, thin, prismatic crystals up to 2–3 cm long. They are formed of compositionally different domains either arranged parallel to the crystal elongation or

https://doi.org/10.1180/minmag.2015.079.5.09 Published online by Cambridge University Press

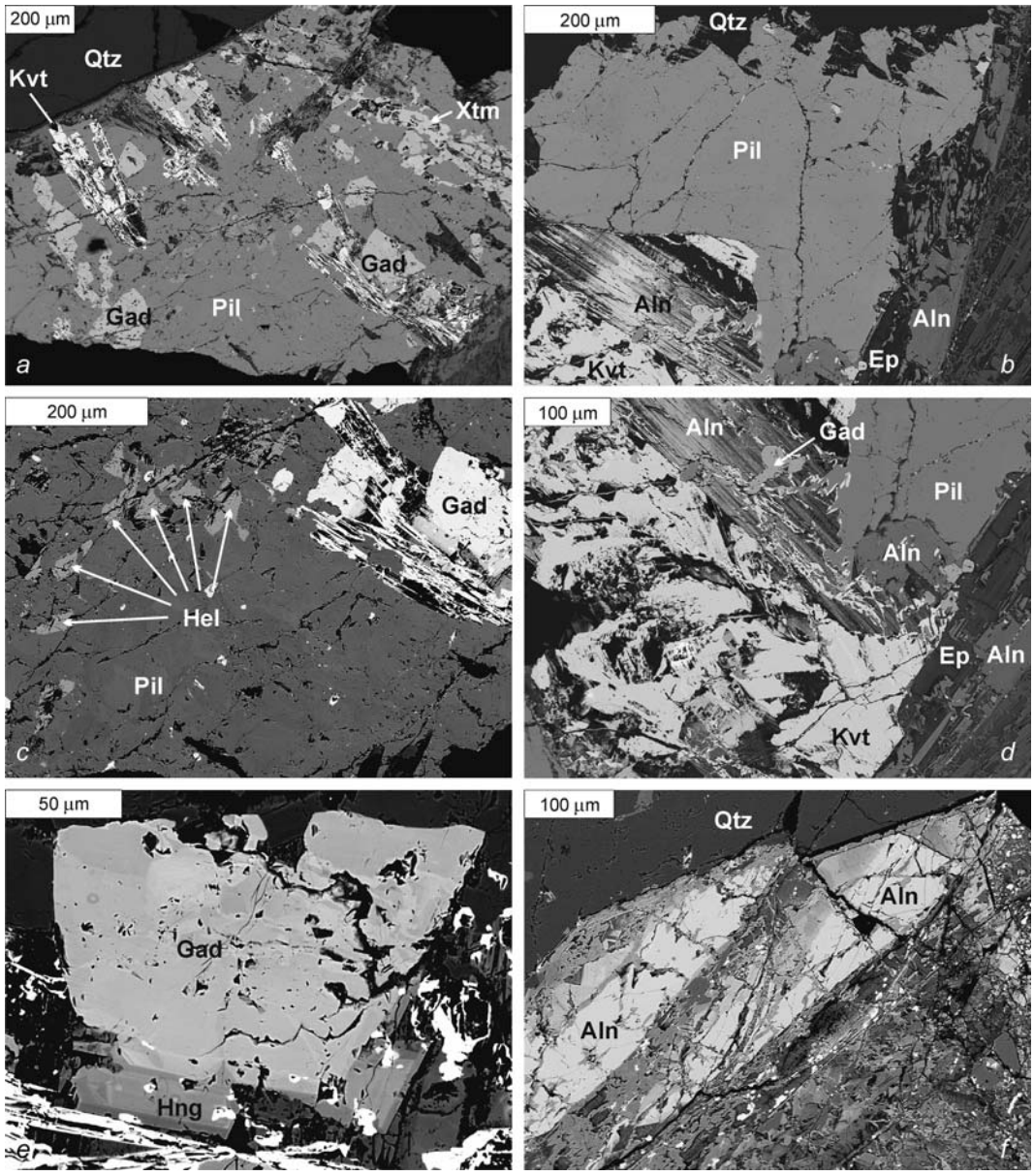

FIG. 1. Backscattered electron images of pilawite-(Y) and associated minerals: (*a*) two intergrown crystals of pilawite-(Y) with numerous inclusions of Y-bearing minerals; (*b*) crystal of pilawite-(Y) used in structural studies; (*c*) internal zoning in pilawite-(Y); (*d*) keiviite-(Y) intergrown with pilawite-(Y); (*e*) an inclusion of gadolinite-(Y) evolving to hingganite-(Y); (*f*) partly altered allanite-(Y). Abbreviations: Aln – allanite-(Y), Ep – epidote, Gad – gadolinite-(Y), Hel – hellandite-(Y), Hng – hingganite-(Y), Kvt – keiviite-(Y), Pil – pilawite-(Y), Qtz – quartz, Xtm – xenotime-(Y).

intergrown randomly. Very often, they are largely altered to unrecognized phases. Crystals closely associated with pilawite-(Y) are commonly enriched in Y and Ln, and represent a crystallization sequence from allanite-(Y), $(Ca_{1.14}Mn_{0.14}Y_{0.55}Ln_{0.14})_{\Sigma 1.97}(Al_{2.18}Fe^{3+}_{0.13}Fe^{2+}_{0.72})_{\Sigma 3.03}[(Si_{2.99}P_{<0.01})_{\Sigma 3.00}$

https://doi.org/10.1180/minmag.2015.079.5.09 Published online by Cambridge University Press

$O_{12}(OH)$, (~70 mol.% of the respective endmember) through transitional members of allanite-(Y) with (Y,Ln)-bearing epidote to epidote or zoisite.

Physical and optical properties

In the investigated sample, pilawite-(Y) occurs as an intergrowth of three anhedral, massive and translucent crystals up to 1.5 mm long. It has white colour and streak, and a vitreous lustre. Neither cleavage nor parting are observed, though irregular fracturing is present. The mineral is brittle and has a hardness of 5 on the Mohs scale. The density, calculated on the basis of molar weight and unit-cell volume, is equal to 4.007 g/cm^3. Pilawite-(Y) is non-pleochroic (colourless in all orientations), biaxial (+), with refractive indices $\alpha = 1.743(5)$, $\beta = 1.754(5)$ and $\gamma = 1.779(5)$, birefringence $\Delta = 0.03–0.04$, $2V_{meas.} = 65(2)°$ and $2V_{calc.} = 68°$. Orientation: X ^ a = 87.5° (β acute), Y // b and Z ^ a = 3.1° (β obtuse).

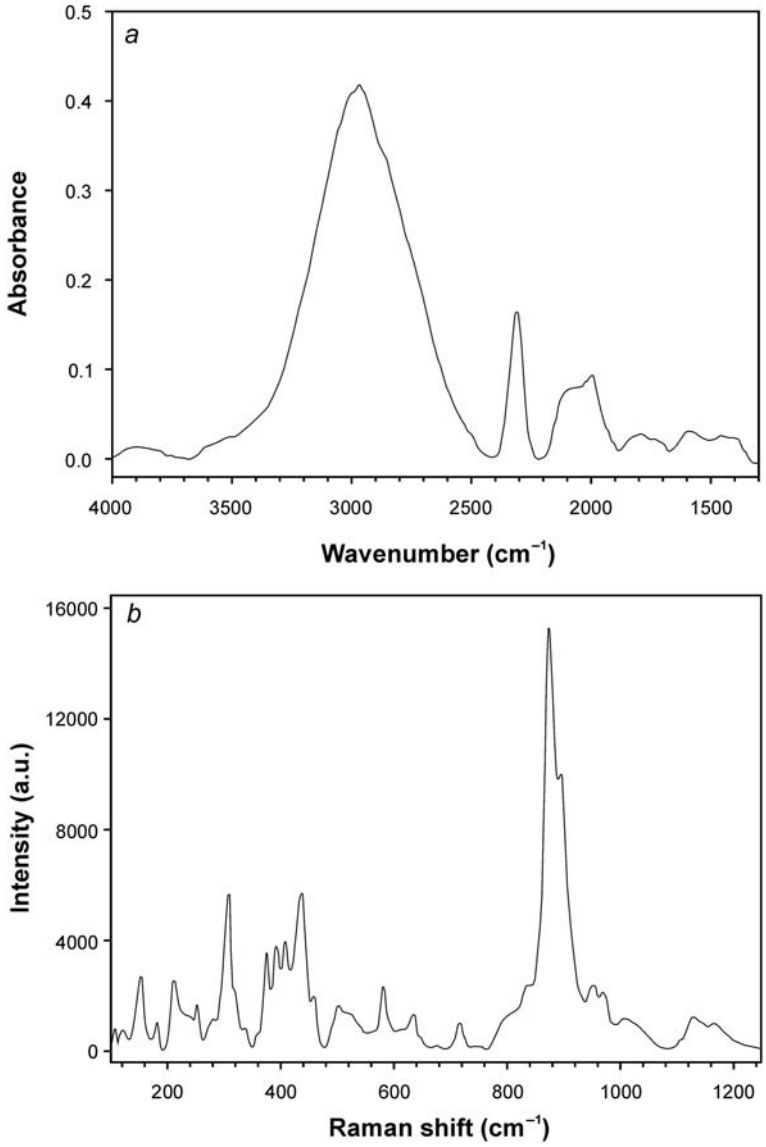

FIG. 2. (*a*) IR spectrum of pilawite-(Y); (*b*) Raman spectrum of pilawite-(Y).

https://doi.org/10.1180/minmag.2015.079.5.09 Published online by Cambridge University Press

Infrared and Raman spectroscopy

The FTIR spectrum shows a broad prominent band at ~2975 cm^{-1}, a sharp band at ~2300 cm^{-1} and a rather ragged weaker doublet centred at ~2050 cm^{-1} (Fig. 2*a*). The band at ~2975 cm^{-1} may be assigned to an O–H stretching mode involving a single OH group in the structure. The wavelength is low because of the high bond-valence incident at the donor O anion: 2 Al + Ca = 1.52 valence units. The weaker band at ~2300 cm^{-1} may be assigned to an O–H stretching mode involving a local arrangement, in which Y replaces Ca at the Ca site.

The Raman spectrum shows prominent Si–O stretching bands in the range ~850–950 cm^{-1} and a large number of Al–O modes and lattice modes below ~600 cm^{-1} (Fig. 2*b*).

Chemical composition

Pilawite-(Y) displays a delicate compositional zoning with irregular cores, visible as lighter domains in backscattered electron (BSE) images, plunged into a darker matrix (Fig. 1*c*). The mean composition of pilawite-(Y) (Table 1) corresponds to the formula $(Ca_{1.88}Mn^{2+}_{0.09}Pb_{0.01})_{\Sigma 1.98}(Y_{1.65}Ln_{0.39})_{\Sigma 2.04}(Al_{3.84}Fe^{3+}_{0.08}Fe^{2+}_{0.04}Ti_{0.03})_{\Sigma 3.99}(Si_{3.98}Al_{0.02}P_{<0.01})_{\Sigma 4.00}O_{18}(OH)_2$. The composition shows (1) a small cation deficiency at the Ca sites and (2) a small surplus of $Y^{3+} + Ln^{3+}$ at the Y sites. A small deficiency of Si is compensated by traces of P^{5+} and Al^{3+}, and as a consequence the <Si(1)–O> and <Si(2)–O> mean bond lengths, 1.632 Å and 1.643 Å, respectively (see later), are somewhat large. The Al(1) and Al(2) octahedra are 96% occupied by Al^{3+} with very minor substitution of Fe^{3+} and Ti^{4+} and completed by Fe^{2+}. However, the dehydroxylation-type substitution $Fe^{3+} + O^{2-} \rightarrow Fe^{2+} + OH^-$ (not taken into account in the formula calculations) can increase the content of Fe^{3+} and the respective sum of Al + Fe^{3+} + Ti to 4 a.p.f.u., excluding completely 2-valent cations at the sites (Mn^{2+} probably substitutes for Ca at the Ca sites). A difference in the <Al(1)–O> and <Al(2)–O> bond lengths, 1.914 Å and 1.936 Å, respectively (see later), suggests substitution of Al^{3+} by Fe^{3+} and Ti^{4+} (and possible Fe^{2+}) mainly at the Al(2) site. Calcium fills the Ca site by ~94%, and its deficiency can be supplemented partly by Mn^{2+} and partly by Y^{3+} + Ln^{3+} and traces of Pb^{2+}. Both main substituents can slightly decrease the observed <Ca–O> mean bond length to the observed value of 2.441 Å. There is always a slight excess of Y + Ln in relation to the two available Y sites in the structure, which corroborates the possibility of limited substitution of Y + Ln for Ca at the Ca site.

Irregular zoning in crystals of pilawite-(Y), observed in the BSE images (Fig. 1*c*), is caused by fractionation of heavy *REE*. However, differences between the Y, Yb, Er and Dy contents in the cores and in the matrix of the pilawite-(Y) crystals are not significant enough statistically to distinguish separate varieties of the mineral. Within the cores, lighter in the BSE images, Y and Er dominate, and they progressively give way mainly to Dy in the matrix material (Fig. 3). Chondrite-normalized *REE* patterns reflect maximum concentration

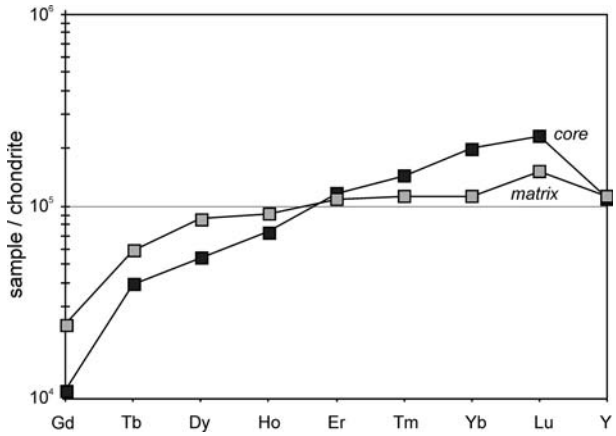

FIG. 3. Chondrite-normalized patterns of pilawite-(Y). Chondritic abundances of Ln and Y are taken from Anders and Grevesse (1989) as 'Mean C1 Chondr.'

https://doi.org/10.1180/minmag.2015.079.5.09 Published online by Cambridge University Press

coefficients of Lu (~$2.5 \cdot 10^5$ times in the cores down to ~$1.3 \cdot 10^5$ in the matrix) > than that of Y (~10^5 times), with progressively decreasing concentrations of successive Ln up to Er (10^5 times), and still more towards Gd (~10^4) and light *REE* with concentrations below the detection limits for WDS determination (~10^3–10^4 times). Generally, Er to Lu decrease from the cores to the matrix, whereas Gd to Ho display an opposite tendency, increasing from ~10^4–$7 \cdot 10^4$ to ~$2.5 \cdot 10^4$–$9 \cdot 10^4$ times, respectively. A compatibility index of the physical and chemical data for pilawite-(Y) = 0.028 places the mineral in the category excellent.

X-ray powder diffraction data and crystal structure

X-ray powder diffraction data

The X-ray powder diffraction pattern is presented in Table 3. The reflections in the pattern were indexed for the monoclinic system, the space-group symmetry $P2_1/c$, on the basis of refined unit-cell parameters $a = 8.558(3)$ Å, $b = 7.260(3)$ Å, $c = 11.182(6)$ Å, $\beta = 90.61(4)^o$, $V = 694.7(4)$ Å^3.

Cation coordination

There are two Si sites, each tetrahedrally coordinated by four O atoms, with only minor variation in the individual Si–O distances (Table 6) and <Si–O> distances of 1.632 and 1.643 Å, respectively. There are two Al sites, each octahedrally coordinated by five O atoms and one (OH) group, each dominated by Al with very minor amounts of Fe^{3+}, Fe^{2+} and Ti^{4+}, and <Al–O> distances of 1.914 and 1.936 Å, respectively. The larger <Al(2)–O> distance of 1.936 Å suggests a small amount of substitution of a larger cation (or cations), and the site scattering at the Al(2) site was refined, giving a refined site-scattering value (Hawthorne *et al.*, 1995) of 26.84(18) electrons per formula unit (e.p.f.u.). This corresponds to a site population at Al(2) of 1.87 Al + 0.13 Fe* (Fe* = Fe^{3+}, Fe^{2+}, Ti^{4+}), in close accord with the analysed chemical compositions for pilawite-(Y). There are two Y sites occupied by Y^{3+} and minor Ln^{3+}, and the sites are separated by 0.59 Å, a distance that is too short for both sites to be locally occupied. The Y(2) site has an occupancy of only 0.044(3) Y^{3+} + Ln^{3+}. The Y(1) site is [8]-coordinated with Y–O distances in the range 2.17–2.66 Å and a <Y(1)–O> distance of 2.408 Å; the Y(2) site is [6]-coordinated with Y–O distances in the range 2.11–2.58 Å and a <Y(2)–O> distance of 2.314 Å. The Ca site is [7]-coordinated by O atoms with a <Ca–O> distance of 2.441 Å. Site-scattering refinement gave a refined site-scattering value of 45.01(19) e.p.f.u., indicating that the Ca site is dominated by Ca but also that there is considerable substitution of a heavier cation for Ca. The chemical analytical data for pilawite-(Y) indicate a deficiency of Ca (~1.88 Ca a.p.f.u.) relative to the site sum of 2 a.p.f.u., and the presence of Mn and very minor Pb (0.007 a.p.f.u.) that was assigned to this site. However, this gives a calculated site-scattering value of < 41 e.p.f.u., compared to the refined value of 45 e.p.f.u. It is apparent that there is some disorder of Ca and (Y,Ln) between the Ca and Y sites. We cannot calculate an accurate value for the amount of this disorder because of the variation in the scattering factors of Y and Ln. However, we may provide limits on the possible site populations for the Ca site: they will range between Ca = 1.74 Ca + 0.26 Y and Ca = 1.88 Ca + 0.12 *REE*.

Hydrogen bonding

The single H atom was located in the final stages of refinement, and is ~0.98 Å from the O atom (subsequently) labelled OH. The H atom forms a

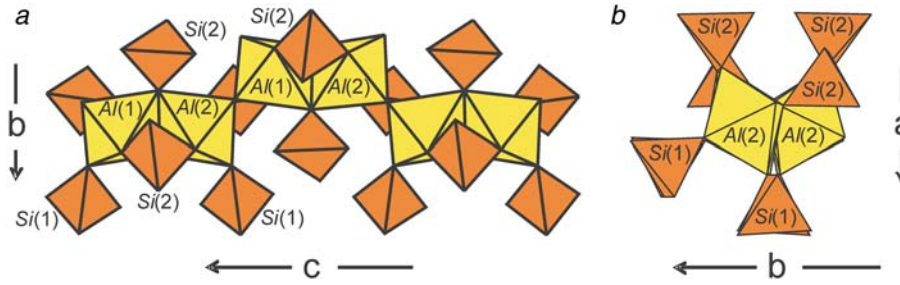

FIG. 4. The $[Al_2(SiO_4)_4\varphi_2]$ decorated chain in pilawite-(Y): (*a*) viewed approximately down *a*; (*b*) viewed 'end-on'; yellow: Al octahedra; orange: Si tetrahedra.

https://doi.org/10.1180/minmag.2015.079.5.09 Published online by Cambridge University Press

hydrogen bond with the O(6) anion at a distance of 1.65 Å and an O–H···O(6) angle of 167°. The OH···O(6) distance, 2.614 Å, corresponds well to 2.644 Å as a d(O···O) distance of the hydrogen bond calculated on the basis of the correlation function established by Libovitzky (1999) and the wavenumber of the main O–H stretching mode at 2975 cm^{-1}. Such a value of the donor–acceptor distance suggests strong hydrogen bonds in pilawite-(Y).

Bond topology

The Al(1) and Al(2) octahedra share an edge to form an $[Al_2\varphi_{10}]$ dimer. This dimer shares corners with other dimers (Fig. 4*a*) to form a chain extending along the *c* axis. Two apical vertices of each dimer are linked by a Si(2) tetrahedron, and apical vertices of adjacent dimers are linked by a Si(1) tetrahedron (Fig. 4*a*,*b*), and the chain is further decorated by tetrahedra that also link to adjacent chains. The overall stoichiometry of the chain is $[Al_2(SiO_4)_4\varphi_2]$. The offsetting of the dimers of octahedra (Fig. 4*a*) is rather unusual. When viewed down *b* (Fig. 5*a*), the chain of octahedra appears deceptively similar to the common decorated $[M_2O_8]$ chain (e.g. Hawthorne 1985, 1986, 1990). However, careful inspection of Fig. 5*a* shows that adjacent dimers do not share edges, as is the case for the $[M_2O_8]$ chain, but only corners.

These chains link in the *a* and *b* directions (Fig. 6*a*) by sharing corners between octahedra and tetrahedra to form an octahedron–tetrahedron framework with large interstices that contain the Ca^{2+} and $(Y,Ln)^{3+}$ cations.

Comparison with other structures

The $[^{[6]}M_2(^{[4]}TO_4)_4\varphi_2]$ chain occurs in the phosphate minerals palermoite, $Sr_2Li_4[Al_2(PO_4)_2(OH)_2]_2$ (Moore and Araki, 1975) and bertossaite, $Ca_2Li_4[Al_2(PO_4)_2(OH)_2]_2$ (Hatert *et al*., 2011), and the arsenate mineral carminite, $Pb[Fe_2^{3+}(PO_4)_2(OH)_2]$ (Finney, 1963). The chains from pilawite-(Y) and palermoite are compared in Fig. 5*a*,*b*. The chains are topologically identical, although there are minor geometrical differences relating to different space-group symmetries and the different sizes of the (SiO_4) and (PO_4) tetrahedra, and it seems probable that pilawite-(Y) will change symmetry at higher temperature. However, the structures of pilawite-(Y) and palermoite are not topologically congruent, as the $[^{[6]}M_2(^{[4]}TO_4)_4\varphi_2]$ chains cross-link in different ways in the *a* direction. In pilawite-(Y) (Fig. 6*a*), the chains link in a staggered fashion along *a*, emphasized by the thick black lines in Fig. 6*a*. In palermoite (Fig. 6*b*), the chains link in a crankshaft fashion along *a*, emphasized by the thick black lines in Fig. 6*b*. Thus the Al–Si framework of pilawite-(Y) is a graphical isomer of the Al–P framework in palermoite. Pilawite-(Y) and palermoite, bertossaite and carminite are all

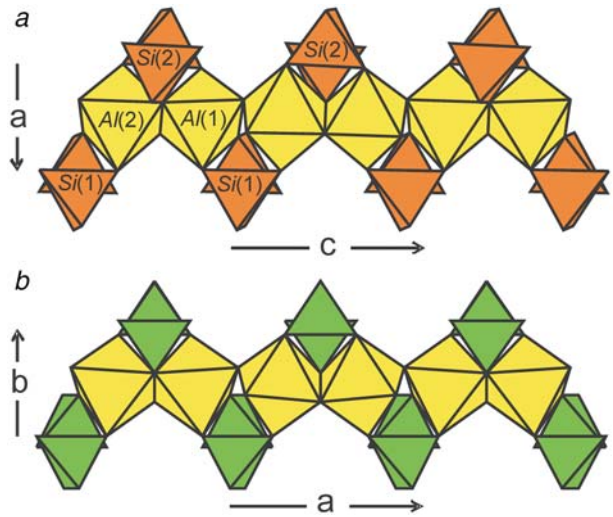

FIG. 5. (*a*) The $[Al_2(SiO_4)_4\varphi_2]$ decorated chain in pilawite-(Y); yellow: Al octahedra; orange: Si tetrahedra; (*b*) the $[Al_2(SiO_4)_4\varphi_2]$ decorated chain in palermoite; legend as in Fig. 4, green: P tetrahedra.

https://doi.org/10.1180/minmag.2015.079.5.09 Published online by Cambridge University Press

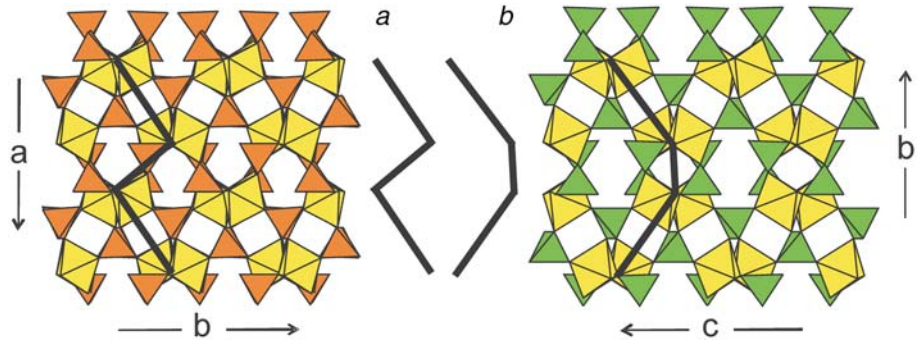

FIG. 6. The octahedron–tetrahedron framework in (*a*) pilawite-(Y) and (*b*) palermoite. The thick black lines emphasize the relative attitudes of the $[Al_2(TO_4)_4\varphi_2]$ chains viewed end-on in each structure; legend as in Figs 5 and 6.

characterized by the presence of strong hydrogen bond(s). However, pilawite-(Y) has only one type of OH group in contrast to the other minerals with structures showing two (palermoite, bertossaite) or three (carminite) such groups. The OH···O distance in pilawite, 2.614 Å, is one of the shortest in the isostructural minerals (palermoite: 2.749(7) Å and 2.845(6) Å, Moore and Araki, 1975; bertossaite: 2.669 Å and 2.629 Å, Hatert *et al*., 2011; carminite: 2.58–2.69 Å, Kharisun *et al*., 1996), and hence has one of the strongest hydrogen bonds in this group.

Origin of pilawite-(Y)

The pilawite-(Y)-bearing dyke belongs to a relatively weakly-fractionated, NYF-affiliated part of the hybrid, NYF + LCT, Julianna pegmatitic system exposed in the Piława Górna quarry (Szuszkiewicz *et al*., 2013). During later stages of solidification, a distinct increase in Ca activity took place, and was perhaps related to early hydrothermal activity recorded in different mineral assemblages (Pieczka *et al*., 2013, 2014). For example, it is apparent in Ca-bearing spessartine replacing primary spessartine, progressive Ca-enrichment of ishikawaite, samarskite-(Y) and polycrase-(Y) and their final alteration to Ca-bearing pyrochlore-supergroup minerals, crystallization of fersmite as well as titanite- and epidote-group minerals, common alteration of beryl to various members of the bavenite–bohseite series, Ca-enrichment in tourmaline, etc. The crystallization of pilawite-(Y) undoubtedly occurred at the same stage of pegmatite evolution, as the mineral is associated with hellandite-(Y), Ca-bearing hingganite-(Y) and epidote-supergroup minerals. The mineral assemblage indicates that crystallization began at high, but decreasing Y + Ln activities and was progressively modified by increasing action of a Ca- and Al-bearing fluid, resulting in the sequence: keiviite-(Y) → gadolinite-(Y) + hellandite-(Y) → pilawite-(Y) → allanite-(Y) → epidote / zoisite.

Acknowledgements

The authors thank members of the IMA CNMNC, Ritsuro Miyawaki, Peter Leverett and an anonymous reviewer for their comments on this manuscript. The studies were supported by the Ministry of Science and Higher Education and the National Science Centre (NCN) grant N N307 241737 and AGH UST grant no 11.11.140.319 to AP and by a Canada Research Chair in Crystallography and Mineralogy, by Natural Sciences and Engineering Research Council of Canada Discovery, Equipment and Major Installation grants and by Innovation grants from the Canada Foundation for Innovation to FCH.

References

Aftalion, M. and Bowes, D.R. (2002) U–Pb zircon isotopic evidence for Mid-Devonian migmatite formation in the Góry Sowie domain of the Bohemian Massif, Sudeten Mountains, SW Poland. *Neues Jahrbuch für Mineralogy, Monatshefte*, **4**, 182–192.

Anders, E. and Grevesse, N. (1989) Abundances of the elements: Meteoritic and solar. *Geochimica et Cosmochimica Acta*, **53**, 197–214.

Bröcker, M., Żelaźniewicz, A. and Enders, M. (1998) Rb–Sr and U–Pb geochronology of migmatitic gneisses from the Góry Sowie (West Sudetes, Poland): the importance of Mid–Late Devonian metamorphism. *Journal of the Geological Society, London*, **155**, 1025–1036.

Brueckner, H.K., Blusztajn, J. and Bakun-Czubarow, N. (1996) Trace element and Sm–Nd "age" zoning in garnets from peridotites of the Caledonian and

https://doi.org/10.1180/minmag.2015.079.5.09 Published online by Cambridge University Press

Variscan mountains and tectonic implications. *Journal of Metamorphic Geology*, **14**, 61–73.

Černý, P. and Ercit, T.S. (2005) The classification of granitic pegmatites revisited. *The Canadian Mineralogist*, **43**, 2005–2026.

Drake, M.J. and Weill, D.F. (1972) New rare earth element standards for electron microprobe analysis. *Chemical Geology*, **10**, 179–181.

Finney, J.J. (1963) The crystal structure of carminite. *American Mineralogist*, **48**, 1–13.

Gordon, S.M., Schneider, D.A., Manecki, M. and Holm, D.K. (2005) Exhumation and metamorphism of an ultrahigh-grade terrane: geochronometric investigations of the Sudetes Mountains (Bohemia), Poland and Czech Republic. *Journal of the Geological Society, London*, **162**, 841–855.

Hatert, F., Lefèvre, P. and Fransolet, A.-M. (2011) The crystal structure of bertossaite, $CaLi_2[Al_4(PO_4)4(OH,F)_4]$. *The Canadian Mineralogist*, **49**, 1079–1087.

Hawthorne, F.C. (1985) Towards a structural classification of minerals: The VIMIVT2φn minerals. *American Mineralogist*, **70**, 455–473.

Hawthorne, F.C. (1986) Structural hierarchy in VIMxIIITyφz minerals. *The Canadian Mineralogist*, **24**, 625–642.

Hawthorne, F.C. (1990) Structural hierarchy in [6]M[4]Tφn minerals. *Zeitschrift für Kristallographie*, **192**, 1–52.

Hawthorne, F.C., Ungaretti, L. and Oberti, R. (1995) Site populations in minerals: terminology and presentation of results of crystal-structure refinement. *The Canadian Mineralogist*, **33**, 907–911.

Kharisun, T.M.R., Bevan, D.J.M. and Pring, A. (1996) The crystal structure of carminite: refinement and bond valence calculations. *Mineralogical Magazine*, **60**, 805–811.

Kryza, R. and Fanning, C.M. (2007) Devonian deep-crustal metamorphism and exhumation in the Variscan Orogen: evidence from SHRIMP zircon ages from the HT–HP granulites and migmatites of the Góry Sowie (Polish Sudetes). *Geodinamica Acta*, **20**, 159–176.

Libovitzky, E. (1999) Correlation of O–H stretching frequencies and O–H···O hydrogen bond lengths in minerals. *Monatshefte für Chemie*, **130**, 1047–1059.

Mazur, S., Aleksandrowski, P., Kryza, R. and Oberc-Dziedzic, T. (2006) The Variscan Orogen in Poland. *Geological Quarterly*, **50**, 89–118.

Moore, P.B. and Araki, T. (1975) Palermoite, $SrLi_2Al_4(PO_4)_4(OH)_4$. Its atomic arrangement and relationship to carminite, $Pb_2(Fe_4(OH)_4(AsO_4)_4$. *American Mineralogist*, **60**, 460–465.

Novák, M. (2005) Granitic pegmatites of the Bohemian Massif (Czech Republic); mineralogical, geochemical and regional classification and geological significance. significance *Acta Musei Moraviae, Scientiae geologicae*, **90**, 3–75 [in Czech with English summary].

Oberti, R., Della Ventura, G., Ottolini, L., Hawthorne, F. and Bonazzi, P. (2002) Re-definition, nomenclature and crystal chemistry of the hellandite group. *American Mineralogist*, **87**, 745–752.

O'Brian, P.J., Kröner, A., Jaeckel, P., Hegner, E., Żelaźniewicz, A. and Kryza, R. (1997) Petrological and isotope studies on Palaeozoic high-pressure granulites. Góry Sowie Mts, Polish Sudetes. *Journal of Petrology*, **38**, 433–456.

Pieczka, A., Szuszkiewicz, A., Szełęg, E., Nejbert, K., Łodziński, M., Ilnicki, S., Turniak, K., Banach, M., Hołub, W., Michałowski, P. and Różniak, R. (2013) (Fe,Mn)–(Ti,Sn)–(Nb,Ta) oxide assemblage in a little fractionated portion of a mixed (NYF + LCT) pegmatite from Piława Górna, the Sowie Mts. block, SW Poland. *Journal of Geosciences*, **58**, 91–112.

Pieczka, A., Szuszkiewicz, A., Szełęg, E., Ilnicki, S., Nejbert, K. and Turniak, K. (2014) Samarskite-group minerals and alteration products: an example from the Julianna pegmatitic system, Piława Górna, SW Poland. *The Canadian Mineralogist*, **52**, 303–319.

Pouchou, I.L. and Pichoir, F. (1985) "PAP" (phi-rho-z) procedure for improved quantitative microanalysis. Pp. 104–106 in: *Microbeam Analysis* (I.T. Armstrong, editor). San Francisco Press, San Francisco.

Reed, S.J.B. and Buckley, A. (1998) Rare-earth element determination in minerals by electron-probe microanalysis: application of spectrum synthesis. *Mineralogical Magazine*, **62**, 1–8.

Sheldrick, G.M. (2008) A short history of SHELX. *Acta Crystallographica*, **A64**, 112–122.

Strunz, H. and Nickel, E.H. (2001) *Strunz Mineralogical Tables, Ninth Edition.* Schweizerbart'sche Verlagsbuchhandlung, Stuttgart, Germany.

Szuszkiewicz, A., Szełęg, E., Pieczka, A., Ilnicki, S., Nejbert, K., Turniak, K., Banach, M., Łodziński, M., Różniak, R. and Michałowski, P. (2013) The Julianna pegmatite vein system at the Piława Górna mine, Góry Sowie Block, SW Poland – preliminary data on geology and descriptive mineralogy. *Geological Quarterly*, **57**, 467–484.

Timmermann, H., Parrish, R.R., Noble, S.R. and Kryza, R. (2000) New U–Pb monazite and zircon data from the Sudetes Mountains in SW Poland; evidence for a single-cycle Variscan Orogeny. *Journal of the Geological Society, London*, **157**, 265–268.

Van Breemen, O., Bowes, D.R., Aftalion, M. and Żelaźniewicz, A. (1988) Devonian tectonothermal activity in the Sowie Góry gneissic block, Sudetes, southwestern Poland: evidence from Rb–Sr and U–Pb isotopic studies. *Journal of the Polish Geological Society*, **58**, 3–10.

Żelaźniewicz, A. (1990) Deformation and metamorphism in the Góry Sowie gneiss complex, Sudetes, SW Poland. *Neues Jahrbuch für Geologie und Paläontologie – Abhandlungen*, **179**, 129–157.

https://doi.org/10.1180/minmag.2015.079.5.09 Published online by Cambridge University Press